THE JOURNAL OF PHYSICAL CHEMISTRY C

Article

pubs.acs.org/JPCC

Alloying, Dealloying, and Reentrant Alloying in (Sub)monolayer Growth of Ag on Pt(111)

Maciej Jankowski,*[,†,‡] Esther van Vroonhoven,[‡] Herbert Wormeester, Harold J. W. Zandvliet, and Bene Poelsema

Physics of Interfaces and Nanomaterials, MESA+ Institute for Nanotechnology, University of Twente, P.O. Box 217, 7500AE Enschede, The Netherlands

Supporting Information

ABSTRACT: An in situ nanoscopic investigation of the prototypical surface alloying system Ag/Pt(111) is reported. The morphology and the structure of the ultrathin Ag−Pt film is studied using low energy electron microscopy during growth at about 800 K. A very rich dynamic behavior is uncovered in which stress relief plays a governing role. Initial growth leads to surface alloying with prolonged and retarded nucleation of adislands. Beyond 50% coverage dealloying proceeds, joined by partial segregation of Pt toward the center of large islands in violent processes. Subsequently, the growing islands coalesce and consequently irregularly shaped vacancy clusters evolve. These clusters are progressively filled by segregating Pt and assume a compact shape (black spots). As a result, at around 85% coverage, the strain of the initially pseudomorphological film is almost completely relieved and Pt segregation is at its maximum. Further deposition of Ag leads to transient reentrant alloying and recovery of the pseudomorphological layer. The black spots persist even in/on several-layer-thick films. Ex situ atomic force microscopy data confirm that these are constituted by Pt(-rich) structures. The (sub)monolayer films are strongly heterogeneous.

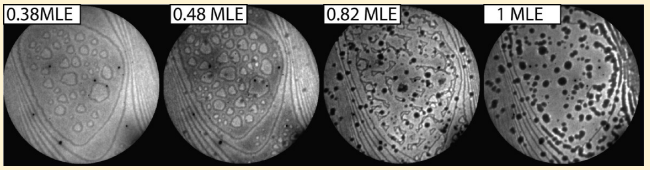

INTRODUCTION

The growth of ultrathin Ag films on Pt(111) has received much attention in the past few decades,[1−7] caused mainly by complex surface alloying[8−10] resulting in the formation of stress stabilized surface nanostructures.[11−14] Interest was further raised by the possibility to generate and tune novel chemical and physical properties by varying the stoichiometry at the surface and careful control of the Ag growth conditions,[14−16] and the formation of periodic dislocation networks[17−20] used as nanotemplates[21] for the growth of organic films.[22−25]

Low-energy electron diffraction (LEED),[2] thermal energy atom scattering (TEAS),[7] and scanning tunneling microscopy (STM)[3] experiments revealed that at room temperature the first Ag layers grew through the formation of large pseudomorphic and thus strained Ag islands. This strain is caused by an about 4% lattice mismatch between the lattice constants of bulk Ag and Pt. An increase of the surface temperature above 550 K leads to irreversible disorder at the surface.[7] STM investigations[8] revealed that this disorder is caused by the formation of a surface confined alloy[13] comprised of strained nanometer-sized Ag-rich structures embedded in the Pt surface.[8] The shape and size of these structures varied strongly with coverage.[11,12,14] After deposition of one monolayer of Ag, the surface was found to be dealloyed and a pseudomorphic Ag layer was formed. Further deposition of Ag induced the formation of a triangular dislocation network which allows relief of the surface strain.[17] The third layer was reported to be a pure silver layer[18] with a propagation of a height undulation originating from the dislocation network at the buried interface.[18−20]

Much important microscopic work on the growth of ultrathin silver films on Pt(111) has been done since this system has become a prototype of surface confined alloying, especially for the heavier transition metal surfaces. However, in situ spatiotemporal information during deposition is still completely lacking. The present study fills this yet unexplored gap. As will be shown, the system shows incredibly rich dynamic behavior which provides important details of the (de)alloying processes in this system. Our investigation reveals that during growth of the first layer at 750−800 K a AgPt surface alloy forms with areas exhibiting a different AgPt stochiometry. Beyond about 0.5 monolayer equivalent (MLE) added Ag, the surface starts to dealloy, which becomes prominent near coalescence of the first layer islands. Further increase of the Ag coverage results in the formation of irregularly shaped vacancy islands which are gradually filled by Pt atoms expelled from the alloy phase. In the last stage, these segregated Pt atoms form compact clusters which are observed as black spots in low energy electron microscopy (LEEM) images. These areas have also been analyzed ex situ with atomic force microscopy (AFM). The combination of these techniques leads to our identification of these black spots as heavily strained and possibly even amorphous Pt features. When the coverage reaches 1 MLE,

Received: November 28, 2016
Revised: March 22, 2017
Published: March 22, 2017

DOI: 10.1021/acs.jpcc.6b11971
J. Phys. Chem. C 2017, 121, 8353−8363

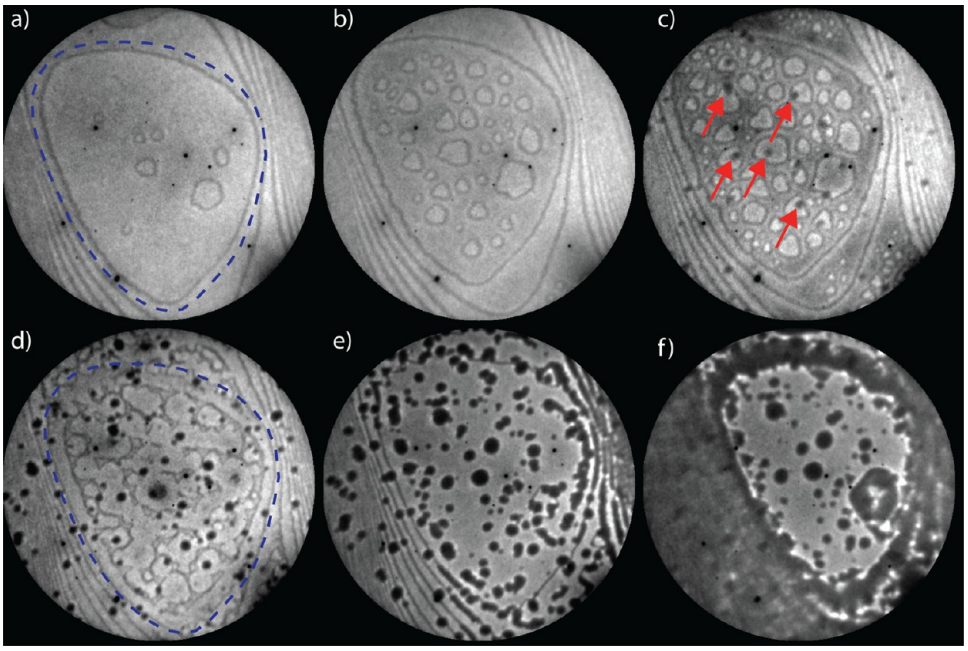

Figure 1. LEEM images recorded in bright-field mode at coverages of (a) 0.275, (b) 0.38, (c) 0.5, (d) 0.76, (e) 1, and (f) 1.25 MLE. The blue contours in (a) and (d) mark the position of the ascending steps for the clean surface bordering the main large terrace in the center as a benchmark. The "ovals", visible in (a) and (b), are the borders of growing first layer islands on the top of the large terrace in the center. The red arrows in (c) point to emerging "black" spots. The results have been obtained with a deposition rate of 1.7×10^{-3} MLE/s. The FoV is 2 μm, the electron energy is 2 eV, and the substrate temperature is 750 K. The small dark spots, best visible in (a), are LEEM channel plate defects. The brightness of each image has been selected individually to enhance morphological details.

we observe that the integral area of these clusters decreases, which is attributed to their partial dissolution caused by a reentrant alloying of the ultrathin Ag film. These "amorphous" Pt clusters are stable upon exposure to atmospheric conditions.

EXPERIMENTAL SECTION

The LEEM measurements were performed with an Elmitec LEEM III with a base pressure better than 1×10^{-10} mbar. The used Pt(111) crystal had a miscut angle of less than 0.1°.[26] Surface cleaning was done by prolonged repetitive cycles of argon ion bombardment, annealing in oxygen at 2×10^{-7} mbar at 800 K, and subsequent flashing to 1300 K in the absence of oxygen. The sample was heated by electron bombardment from the rear, and the temperature was measured with a W 3%/Re–W 25%/Re thermocouple. An Omicron EFM-3 evaporator was used to deposit 99.995% purity silver from a molybdenum crucible onto the sample. The coverage was calibrated on the basis of recorded LEEM movies, where we could track the growth of the first pseudomorphic Ag layer, referenced as 1 MLE and corresponding to 1.5×10^{15} atoms/cm^2, followed by the growth of second layer which propagates from step edges. LEEM images were recorded in bright-field mode using an appropriate contrast aperture around the (00) diffracted beam in the focal plane. The low energy electron diffraction (LEED) patterns were recorded using the largest available aperture of 25 μm in the illumination column.

The AFM measurements were done in air at room temperature with an Agilent 5100 AFM employing amplitude modulation for recording height topography. A MikroMasch Al-black-coated NSC35 Si_3N_4 AFM tip with a tip radius of 8 nm was used in these measurements. The resonance frequency of this tip was 205 kHz, and the nominal spring constant was 8.9 N/m. For the measurements an amplitude set point of 90% and an oscillation amplitude in the range from 30 to 40 nm were used. The amplitude modulation imaging mode provides simultaneously topographic and phase images. The latter provides information on the local variation in energy dissipation involved in the contact between the tip and the sample. Various factors are known to influence this energy dissipation, among which are viscoelasticity, adhesion, and chemical composition.[27]

RESULTS AND DISCUSSION

Overview of Initial Growth and Alloying of Ag on Pt(111); LEEM. Figure 1 shows a sequence of LEEM images recorded during the growth of the first Ag layer on Pt(111) at 750 K (see also Movie S1). The brightness of the various features in these successively recorded images cannot be compared due to the digital enhancement of each individual image in order to always obtain the best contrast settings. An image with a 2 μm field of view (FoV) of the initial Ag deposition on Pt(111) surface is shown in Figure 1a. Figure 1a shows a large terrace in the center, bordered by ascending monatomic steps. Upon deposition the growth of a surface confined alloy is observed, starting from the ascending step edges, the dominant process for narrow terraces,[8] and followed by the nucleation and growth of alloyed islands seen in Figure 1a,b.

As a benchmark the position of the ascending steps bordering the main central terrace is shown in blue for the initial clean surface in Figure 1a,d. In a transient initial stage the steps retract somewhat followed by nucleation of islands on the terrace. The evolving "ovals" show steps of the first layer islands. This very nucleation process, occurring after an initial "ignition" period, already indicates that the adatom mobility

DOI: 10.1021/acs.jpcc.6b11971
J. Phys. Chem. C 2017, 121, 8353–8363

decreases, since not all atoms can effectively reach the ascending steps anymore as was the case initially. This decreased diffusivity is attributed to enhanced diffuse scattering of adatoms on the more heterogeneous potential landscape of the terraces. Reduced diffusivity on an alloyed surface was also described for Co/Cu(001).[28] In the beginning no contrast between the evolving islands and the hosting terrace is visible, which is indicative of similar (or even identical) alloy compositions of both. The Ag atoms arriving "far" from the steps will have a finite probability to be incorporated in a surface vacancy. Using the experimentally obtained formation energy for Pt(111) vacancies of 0.62 ± 0.06 eV,[29] we find a vacancy concentration of 10^{-5}–10^{-4}. Therefore, ready surface alloying will take place already from the very start of the deposition. (Note that an atom that arrives near the center of the large terrace has to travel a linear distance of about 4000 lattice sites to reach a step.) See also the Supporting Information.

Beyond a Ag coverage of roughly 0.5 MLE [Figure 1c] the surface dealloys[11] slowly and the islands start to coalesce. During the dealloying phase the surface is quite heterogeneous, especially, but not exclusively, on top of the largest islands. Darkish or "black" spots [marked by red arrows in Figure 1c] develop first in the center of the adatom islands and later at an enhanced rate during coalescence. The black dots reveal Pt segregation which we focus on in this paper, not only on the process but also on its physical origin. At 0.75 MLE, coalescence of the islands leads to formation of elongated vacancy clusters [meandering "lines" in Figure 1d]. With continuing Ag deposition these vacancy clusters are filled by expelled Pt atoms, and at 1 MLE [Figure 1e] they then take compact shapes as we will detail further below. Completion of the monolayer leads to a decrease of the integral exposed area of the black dots. This shrinkage of the dots is accompanied by a reduced total brightness and indicates reentrant alloying. The second layer starts to grow by step propagation [see Figure 1f] and island nucleation in the centers of terraces.

To illustrate the evolution of the Pt segregation, we plot in Figure 2 the fractional area of the black spots as a function of the coverage. The initial increase of the area, up to 0.8 MLE, is caused by development of the black spots in the centers of the islands. Later, the steep increase, at around 0.85 MLE, is related to the filling of the vacancies by Pt atoms at an enhanced rate, which is followed by a distinct decrease just before completion of the first layer. This decrease reveals the partial dissolution of the black spots due to the reentrant alloying of the film when approaching completion of the first monolayer.

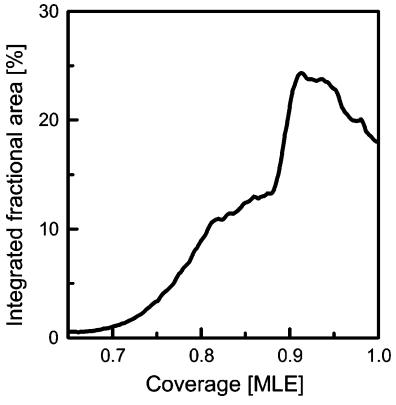

Figure 2. Integrated fractional area of the black spots vs coverage. The fractional area is calculated from the images recorded with 4 μm FoV.

Mixing in Initial Submonolayer Growth of Ag on Pt(111); LEEM. Figure 3 shows representative snapshots of a movie taken during the initial growth of Ag/Pt(111). The brightness of the exposed layer decreases immediately after opening of the Ag evaporator shutter. This is indicative of an increase of the diffuse scattering due to alloying related disorder[7] and will be discussed in more detail in the section Dealloying of the Alloy above 0.5 MLE; LEEM. It is also obvious that at first the material is accommodated at the ascending steps. These steps propagate downward toward the large terrace in the center. Initially effectively all materials, i.e., the excess Ag atoms and the Pt atoms expelled from the exposed surface, are sufficiently mobile to reach the preexisting steps. During these initial stages the brightness of the surface is identical everywhere indicating that the emerging surface undergoes alloying in which the Ag embedded in the surrounding Pt matrix[8,11,12] is homogeneously distributed. There is also no brightness variation on the narrower terraces near the outer skirts of the images. After some incubation time at about 0.3 MLE a few islands, visible in Figure 3b, nucleate in the central region of the large lower terrace. This provides another indication of a peculiar, alloying related feature. Where initially the mobility was sufficiently large for the atoms to reach the bordering steps, the actual mobility becomes insufficient to reach the propagating steps even if their separation has decreased. This is the first indication for a decreasing mobility of (Pt and Ag) adatoms on the alloying surface. Between panels c and d of Figure 3 the first layer coverage has increased from 0.48 to 0.7 MLE and consequently dealloying occurred. This

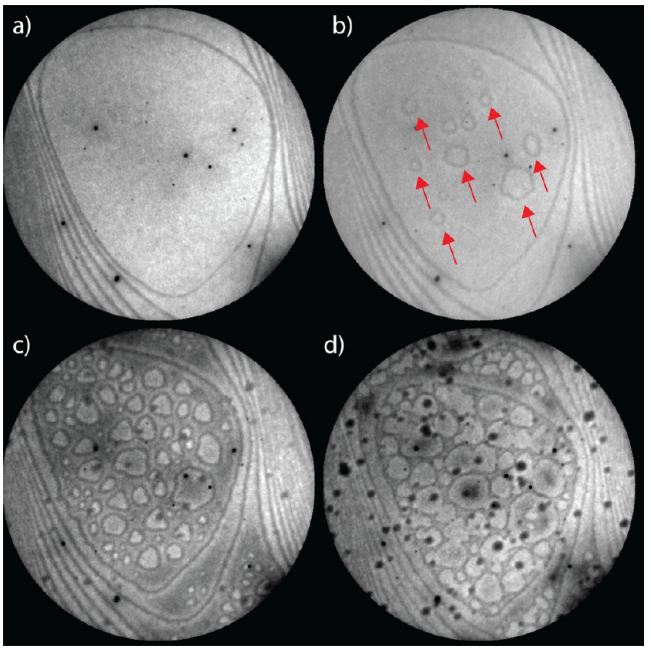

Figure 3. LEEM images recorded in bright-field mode: (a) clean Pt(111), (b) 0.3 MLE, (c) 0.48 MLE, and (d) 0.7 MLE. The red arrows in (b) point to few nucleated alloy islands. The results have been obtained with a deposition rate of 1.7×10^{-3} MLE/s. The FoV is 2 μm, the electron energy is 2.0 eV, and the substrate temperature is 750 K. The small dark spots, best visible in (a), are LEEM channel plate defects. The brightness of each image has been selected individually to enhance morphological details.

DOI: 10.1021/acs.jpcc.6b11971
J. Phys. Chem. C 2017, 121, 8353–8363

leads to now an increased mobility and thus the absence of significant new nuclei and the further growth and coalescence of the existing islands.

As one can notice, the number of islands increases up to late stages of growth as illustrated in Figure 4, where we plotted the

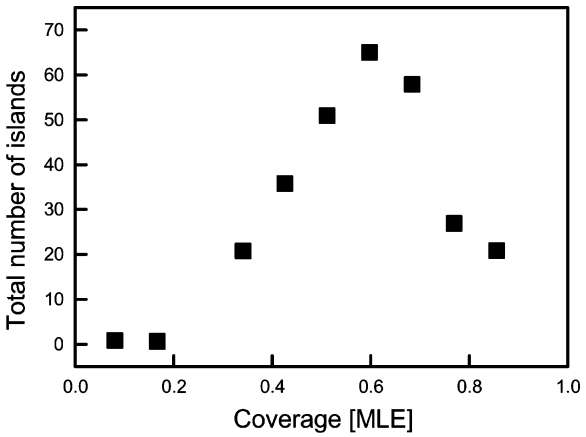

Figure 4. Number of first layer islands as a function of deposition time. The deposition rate is 1.7×10^{-3} MLE/s.

number of islands as a function of time. Progressive nucleation takes place, which leads to a peak in the island density at an unconventionally high coverage of 0.64 MLE.

Another way of illustrating the late nucleation behavior is depicted in Figure 5: unlike in conventional nucleation and growth, where nucleation is about finished after deposition of 1% of a monolayer and the emerging islands keep growing with a quite narrow size distribution, until they coalesce.[30] In the present case nucleation still is active at 0.64 MLE. Moreover, the island size distribution is extremely broad and positional distribution is all but homogeneous. The smallest islands, which have nucleated late, emerge near the atomic steps in the originally denuded zone.

A straightforward explanation for the combined observations, presented in Figures 4 and 5, is alloying in the two exposed levels. Due to the progressive heterogeneity of the top layer, the effective diffusion length decreases continuously and dramatically. As a result, enhanced late nucleation takes place. In a site hopping framework one would conclude that the activation energy for diffusion increases by not less than a factor of 4. One safely arrives at the conclusion that initially the mobility of the adatoms decreases with increasing coverage. However, an attempt to nail this down to more definite numbers will fail due to the complexity of the system.[28] The diffusing species are both Ag atoms and expelled Pt atoms, and these move across a heterogeneous top layer with small Ag-rich patches embedded in the Pt matrix. Moreover, with increasing coverage the concentration of embedded Ag atoms increases, while in a site hopping model the residence times on top of Ag filled sites and on top of Pt filled sites will most likely be different for diffusing Ag atoms and Pt atoms. One cannot exclude either that exchange processes further slow down the diffusion rates. We note that the demixing occurring at higher coverage leads to a more homogeneous composition and, as a consequence of reversing the argument, to enhanced diffusion and thus exclusion of new nucleation events. During these late stages of monolayer growth the number of islands also decreases as a result of coalescence processes.

Dealloying of the Alloy above 0.5 MLE; LEEM. A striking feature is the emergence of black spots as shown in Figure 6. The black spots do appear when approaching

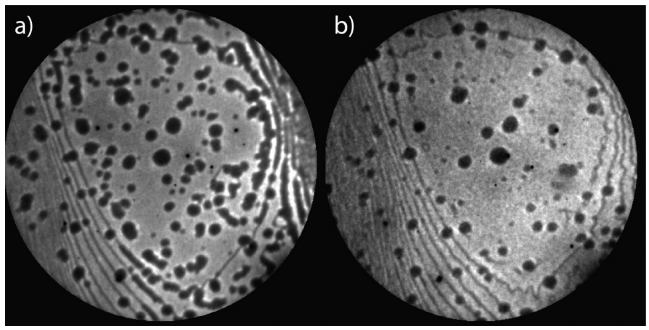

Figure 6. LEEM images recorded in bright-field mode: (a) 1.0 and (b) 1.68 MLE. The results have been obtained with a deposition rate of 1.7×10^{-3} MLE/s. The FoV is 2 μm, the electron energy is 2.0 eV, and the substrate temperature is 750 K. The brightness of each image has been selected individually to enhance morphological details.

completion of the monolayer and are emerging in Figure 3c. They persist after the growth of several monolayers, and are even visible after the completion of the eighth monolayer (not shown here). We have carefully tried to identify their origin. For this purpose we have varied the deposition rate between 1.7×10^{-4} and 1.1×10^{-2} MLE/s. Both the number density of black dots and their integrated area are at variance with the anticipated behavior for contamination: both increase a few tens of a percent, i.e., much less than the factor 65, which might be anticipated from the ratio of the exposure times of the Pt surface layer (which is by far more reactive than Ag). Occasionally, we do observe some evidence of carbon

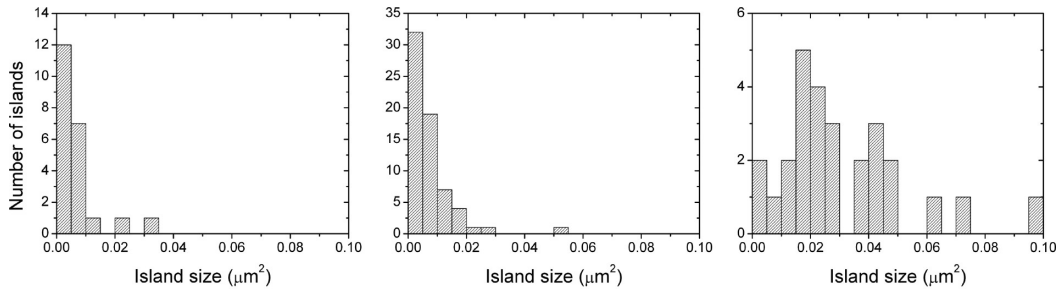

Figure 5. Island size distribution for various submonolayer coverages of 0.30, 0.45, and 0.60 MLE presented in (a), (b), and (c), respectively.

DOI: 10.1021/acs.jpcc.6b11971
J. Phys. Chem. C 2017, 121, 8353−8363

impurities (not visible in presented LEEM figures). However, their signature as a result of creating underfocus and overfocus conditions differs completely from that of the black dots in Figures 3 and 6. We therefore conclude that the "black spots" are inherent to the Ag−Pt(111) demixing process. They appear to consist of disordered Pt-rich patches which reduce in integral size with increasing film thickness, but persist even after deposition of 8 MLE.

Figure 7a shows the evolution of what naively would be called the uncovered area, i.e., the supposedly still exposed

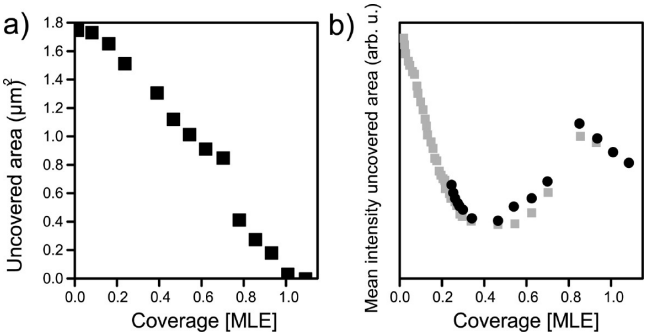

Figure 7. (a) Growth process of Figure 3 analyzed in the uncovered area (see text). (b) Mean bright field intensity as a function of time. The exposed top layer of the substrate is represented by squares; the exposed first layer is represented by circles. The area taken by black spots is subtracted from the analysis. The break above 0.75 MLE is caused by not-well-defined morphology of the surface caused by rapid dealloying which causes big uncertainties in the performed analysis. Imaging electron energy is 2 eV.

virgin Pt(111) surface. As we will see shortly, this conjecture cannot be maintained. The area taken by the black dots has been subtracted. Within the uncertainties originating from this subtraction and/or from lensing effects as a result of field irregularities due to e.g. work function differences, the "exposed Pt" area decreases linearly with time, indicative of the growth of a single layer. More information is obtained from the averaged brightness of the layers evolving at the two exposed levels as shown in Figure 7b. In this evaluation the black dots have been disregarded. The gray symbols refer to the original level of the clean Pt(111) surface, while the black circles represent the results for the exposed surface at a coverage that is one monolayer higher. As becomes immediately evident, the brightness decays strongly from the very start of the deposition. It passes through a pronounced minimum and subsequently increases again up to a maximum value after deposition of roughly 0.85 MLE (as we will explain below, this maximum brightness marks busy activity in demixing, segregation, stress relaxation and reentrant mixing). It is also obvious that the average brightnesses of both exposed layers are very similar. Both observations are completely consistent with the formation of a mixed adlayer, or the surface confined alloy discussed in refs 8, 11, and 12. Alloying proceeds during the deposition of the first half-layer, while dealloying occurs during deposition of the second half-monolayer. The alloy can only persist in the vacuum exposed layer(s) due to the involved energetics. First the tensile tension in the Pt(111) is reduced by the incorporation of the larger Ag atoms,[13] while with increasing Ag content the tension finally becomes compressive, which leads to the exchange of first layer Pt with Ag embedded in the lower layer. In the initial phase the brightness decays due to increasing disorder by the continuing embedding of Ag patches in the Pt matrix, while later on the demixing leads to lesser disorder: the continuing expulsion of Ag leads to larger Pt patches surrounding the embedded Ag.

The brightness across the level of the growing adlayer is by no means homogeneously distributed during the growth beyond about 0.40 MLE. A representative snapshot is shown in Figure 3c. At the chosen imaging conditions the smaller islands are bright, the ones with "intermediate" sizes are slightly less bright, many of them have a distinct black dot, and some of them have a distinctly brighter rim, when compared to their centers. This feature is even clearer for the largest islands, which all have a bright rim and a dimmer central part. We interpret these findings as follows: the brighter areas represent Ag(-rich) areas. The smaller islands which appear during late stages of the nucleation are constituted by Ag atoms which are still continuously deposited and Ag atoms which are now expelled from the initial level, i.e., from the alloyed exposed parts of the substrate. During later stages of growth of the intermediately sized and largest islands, the edges also accommodate mostly Ag atoms for the same reason. The resulting bright rims appear to have a characteristic width which does not depend on the island size. The results obtained for a number of islands from several deposition experiments are shown in Figure 8. The distribution of the widths of these

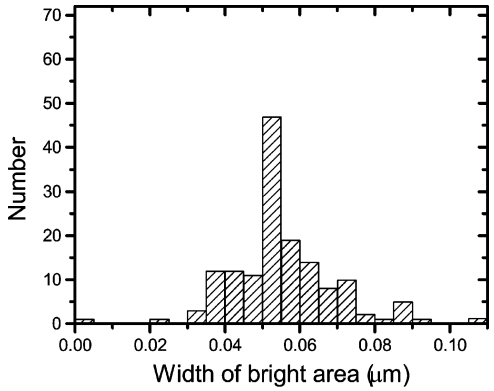

Figure 8. Histogram of widths of the bright borders of the large islands obtained from several experiments.

bright rims/borders is somewhat skewed but has a pronounced maximum at about 52 nm. These widths show no distinct correlation with island size or deposition rates which suggests a thermodynamic origin. We attribute this to the relaxation of stress. The compressed Ag film can best (partly) relieve its stress near the descending step edges. The emergence of bright rims is responsible for the slightly higher brightness obtained for the highest layer around 0.5−0.68 MLE in Figure 7b.

With increasing silver deposition the demixing of the surface confined Ag/Pt alloy continues. The expulsion of surplus Ag from the lower level, i.e., the original substrate level, is apparently facilitated by the advancing steps. However, the Pt atoms, encapsulated on the intermediate and, in particular, on large islands lack that opportunity and experience difficulties to escape. Therefore, these centers remain relatively dark during a prolonged period. Upon demixing, also the larger islands become brighter, the segregation intensifies, and dark gray spots evolve, signaling segregation. On the largest islands, the dimmer inner parts are also Pt-rich and strong fluctuations occur as evidenced in Figure 9. The dark gray areas fluctuate

DOI: 10.1021/acs.jpcc.6b11971
J. Phys. Chem. C 2017, 121, 8353−8363

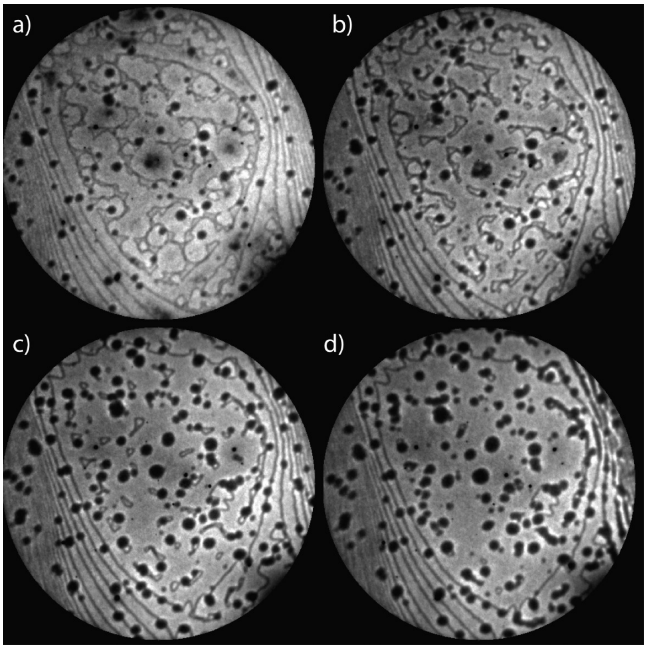

Figure 9. LEEM images recorded in bright-field mode: (a) 0.75, (b) 0.82, (c) 0.88, and (d) 0.95 MLE. The results have been obtained with a deposition rate of 1.7×10^{-3} MLE/s. The FoV is 2 μm, the electron energy is 2.0 eV, and the substrate temperature is 750 K. The brightness of each image has been selected individually to enhance morphological details.

strongly both in position and in brightness. Finally, also the largest islands host dark gray spots [cf. Figure 3d taken at a coverage of 0.7 MLE]. We note that at the same time the brightness of the small islands is unaffected. Some of the dark gray areas evolve into dark spots, while others seem to dissolve again in the Ag layer. Around a total Ag coverage of 0.85 MLE, i.e., during late stages of coalescence, an enormous bustle is taking place. The irregularly shaped vacancy clusters, which are the result of the continuing growth of the coalesced islands, are with an overwhelming majority filled by segregation of Pt into black dots [see Figures 9c,d and 10]. At the same time the brightness of the large islands has now reached its maximum [see Figure 7b]. This late and strikingly active stage of the birth of new Pt-rich dots happens precisely in those areas where the step advancement ceases. This filling of the irregularly shaped vacancy islands with black Pt dots goes along with a strong reduction of their integrated border length, since all dots are circular in shape. The energetically unfavorable long integrated step length apparently facilitates the Pt segregation after which a much reduced domain border length surrounds the circular black spots. Both features are quantified and illustrated in Figures 10 and 11.

We stress that we did carefully look for indications of structures in the recorded micro-LEED (μLEED) patterns during Ag deposition, different from the pseudomorphic (1 × 1) structure, and did not observe any evidence for those. At this same time, as we will show in a moment, we observe relaxations of the surface lattice which reaches a maximum at 0.85 MLE (see Figure 13), the coverage where the brightness of the islands reaches a maximum in Figure 7b. We therefore must conclude that these black dots are possibly amorphous Pt(-rich?) areas. Further support for this conclusion is provided by their circular shape: The Pt-rich dots are heavily strained in their Ag-rich environment and undergo strong and isotropic,

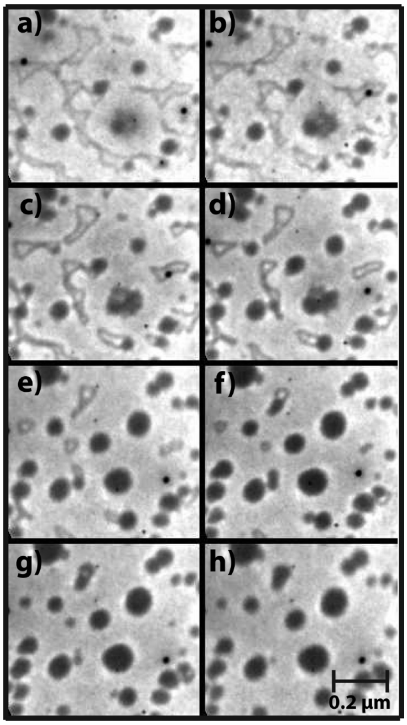

Figure 10. LEEM images recorded in bright-field mode at coverages of (a) 0.75, (b) 0.79, (c) 0.82, (d) 0.85, (e) 0.89, (f) 0.92, (g) 0.96, and (h) 1 MLE. The results have been obtained with a deposition rate of 1.7×10^{-3} MLE/s. The electron energy is 1.9 eV.

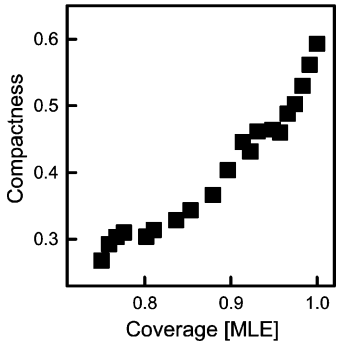

Figure 11. Plot of vacancy compactness as a function of coverage.

compressive stress. In a later stage some even coalesce and become larger, eventually resuming their circular shape. We observe that the decrease of the size of the vacancies goes along with a change of their shape to a more compact one. This shape evolution can be seen in Figure 11 which shows the compactness of the vacancies as a function of coverage. The compactness C is defined as

$$C = \frac{(4\pi A)^{1/2}}{P} \quad (1)$$

where P is the perimeter of vacancies and A is their area.

At 0.85 MLE presented in Figure 10d, the expelled Pt atoms start to segregate into the vacancies, which finally at 1 MLE [see Figure 10h] leads to their complete filling. We note two more things: First with increasing compactness the length of the energetically less favorable edges decreases. Also the step energy will be lower in contact with platinum compared to a vacancy. Both features lead to a lowering of the total free

DOI: 10.1021/acs.jpcc.6b11971
J. Phys. Chem. C 2017, 121, 8353−8363

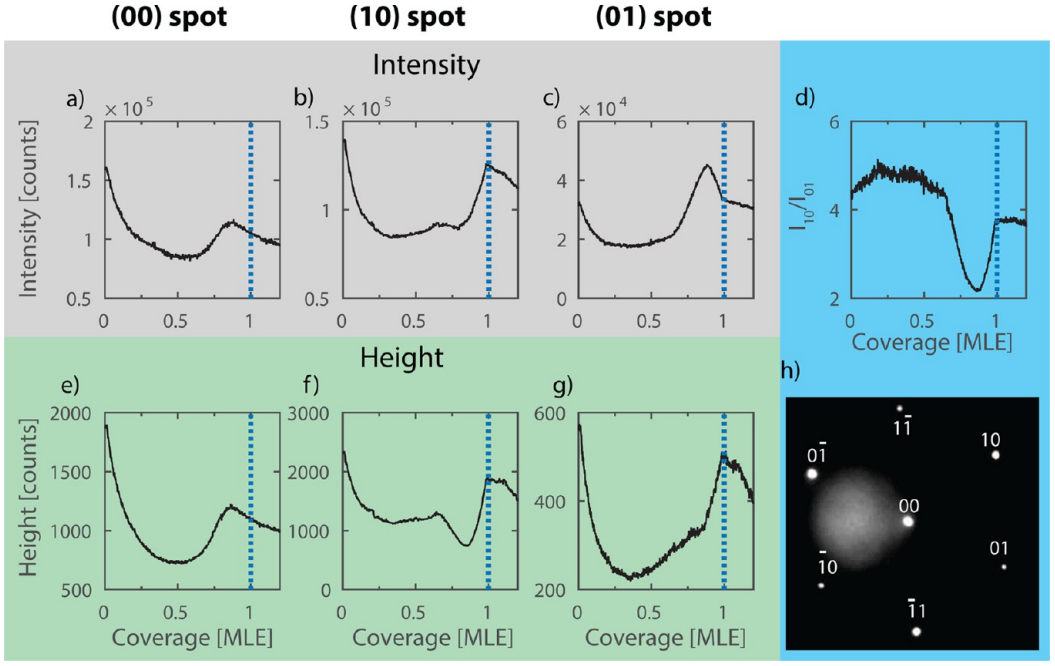

Figure 12. Intensity of LEED spots as a function of coverage: (a) (00) spot, (b) (10) spot, and (c) (01) spot. Height of the LEED spots as a function of coverage: (e) (00) spot, (f) (10) spot, and (g) (01) spot. Blue line marks completion of the first monolayer. (d) Ratio of (10) and (01) spot intensities as a function of coverage. (h) Typical LEED pattern recorded from clean Pt(111) with labeled position of corresponding spots. The results have been obtained with a deposition rate of 1.7×10^{-3} MLE/s. The electron energy is 44 eV, and the sample temperature is 800 K.

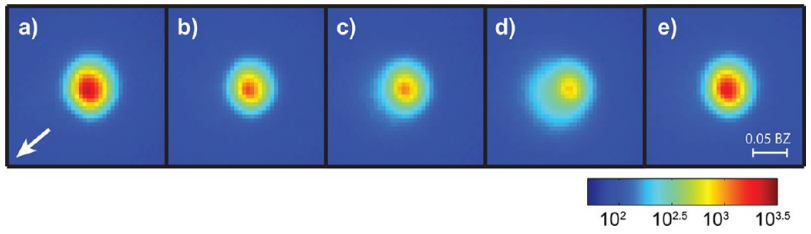

Figure 13. (01) LEED spot recorded during growth of Ag on Pt(111) at 800 K: (a) clean Pt(111), (b) at 0.65 MLE, (c) at 0.74 MLE, (d) at 0.85 MLE, and (e) at 1 MLE. The arrow in (a) points the direction toward the (00) spot. The energy of electrons was 44 eV. The intensity of the spots is presented on a logarithmic scale of colors.

energy and thus facilitate the Pt segregation. In other words, under heavy compressive stress the exposed Pt atoms actually experience an energetic advantage by segregation into the compacting vacancies. We note that, as illustrated in Figure 11, the compactness never seems to reach its ideal value of 1. Uncertainties related to field distortion effects[31] play an uncertain role and make the derivation of a meaningful quantitative number for the compactness hazardous, and we stay away from this path. The qualitative increase of the compactness with coverage is well secured.

LEED Spots Intensity Variation and Surface Lattice Relaxation. The surface lattice variation can be studied in detail from the evolution of the in situ μLEED patterns recorded as a function of Ag coverage. In the initial phase of Ag deposition, surface alloying induces the sharp decrease of the intensity of the Bragg spots[7,19] shown in Figure 12, but their position corresponding to the Pt(111) lattice [Figure 13] is not altered. At around 0.7 MLE, where coalescence of islands and nucleation of well-defined black spots in their centers are observed, the intensity of the (01) spots decreases to reach a local minimum at 0.85 MLE. At this same coverage, the (01) spot intensity reaches a maximum and both first order spots broaden slightly toward the (00) spot, as shown in Figure 13c. We attribute this broadening to the relaxation of the surface lattice toward the 4% larger Ag distances. This relaxation of the lattice is triggered by dealloying of the surface and partial segregation of Pt into vacancy clusters as discussed above. Moreover, the value of the (10)/(01) spot intensity ratio plotted as a function of coverage in Figure 13d reaches a minimum at exactly 0.85 MLE. This is a direct result of a transient lowering of the 3-fold symmetry: The Ag atoms in the relaxed film occupy not only fcc sites but also hcp sites. The latter contribute to enhanced 6-fold symmetry features.

The first monolayer is pseudomorphic, as its observed $p(1 \times 1)$ LEED pattern given in Figure 13e corresponds to that of the Pt(111) lattice.[2,7,19] We also mention that after reaching 0.85 MLE the intensity of the (00) spot in Figure 13a again decreases, which rationalized as reentrant mixing of the top layer. This is in line with the partial dissolution of the black spot [cf. Figure 2] and the concomitant decrease of the brightness of exposed layers [Figure 7b]

We now focus on the nature of the black spots and apply different techniques for their characterization. The latter include spatially resolved work function (WF) measurements with LEEM and ex situ AFM data. The latter provides support

DOI: 10.1021/acs.jpcc.6b11971
J. Phys. Chem. C 2017, 121, 8353−8363

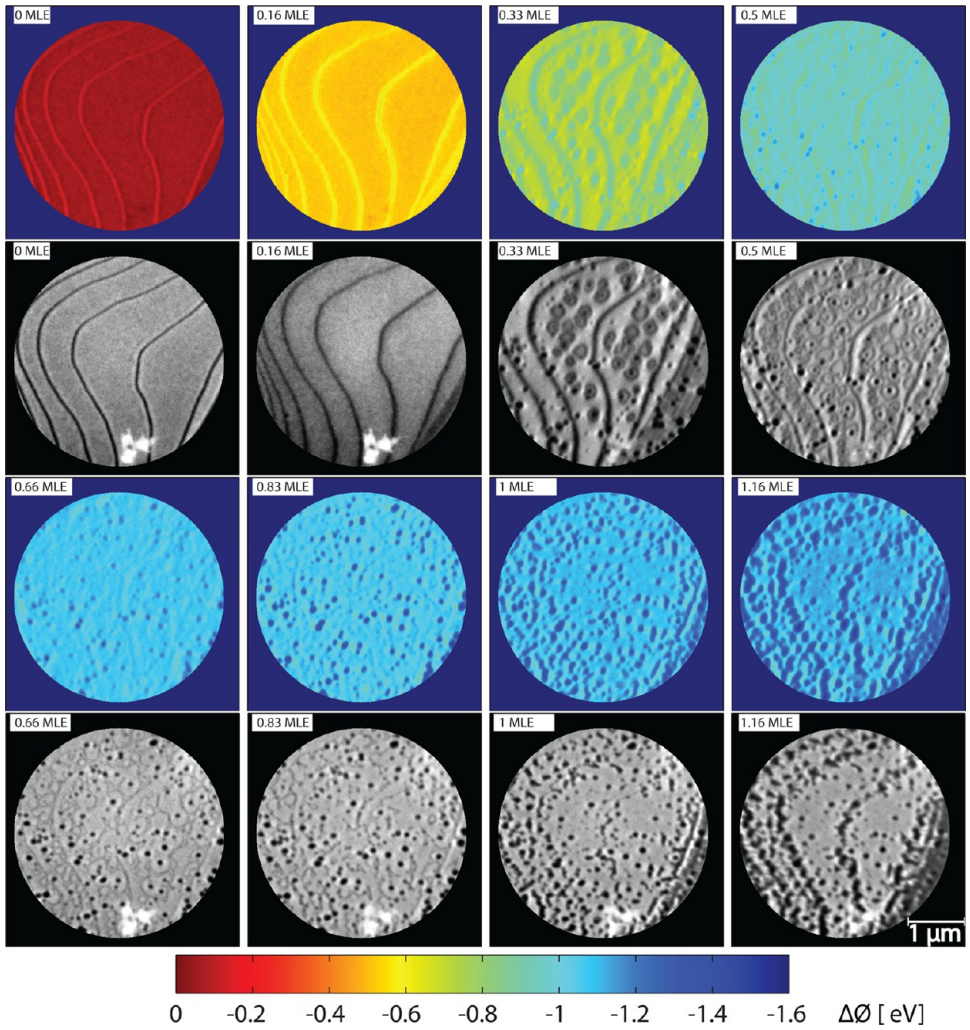

Figure 14. LEEM images recorded in bright-field mode at indicated silver coverage (gray scale color) and concomitant change in WF relative to clean Pt(111) (color scale images). The results have been obtained with a deposition rate of 5.5×10^{-4} MLE/s. The change in the WF is measured with the accuracy of ±0.023 eV.

for the conclusion that excreted Pt atoms constitute the black dots.

Work Function Changes. The LEEM offers the capability of recording spatial maps of relative changes of the surface WF change (see ref 20 for details) during deposition of thin films. To obtain the spatial maps of the WF changes, we measured the brightness of individual pixels as a function of the electron energy and the local WF corresponding to each pixel was derived using the method described in ref 20. The WF change was then obtained from the difference between the local WFs for the clean surface and the Ag-covered surface. Figure 14 shows a sequence of LEEM images and the corresponding spatial maps of the surface WF change as a function of deposition time. The atomically clean terraces of Pt(111) exhibit a constant value of the WF and only a 0.2 eV lower WF is seen at the step edges.[32] The initial deposition of Ag leads to a sharp decrease of the average WF, shown in Figure 15. After 10 min of Ag deposition (at around ~0.3 MLE) the WF of the growing islands ($\Delta\phi$ = −0.79 eV) is 0.1 eV lower than the WF of the surrounding hosting terrace ($\Delta\phi$ = −0.69 eV). This contrast in WF is attributed to different levels of intermixing of Ag and Pt in the islands and their surroundings. The work function has been measured also above the black spots,

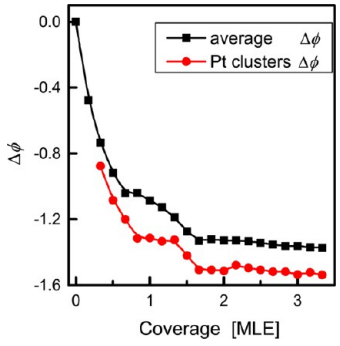

Figure 15. Average and Pt cluster work functions as a function of coverage.

assumed to be Pt(-rich) clusters. As shown in Figure 15, the latter follows quite closely the WF variation of their environment at a distance of about −0.2 eV. The similarity in temporal dependence makes sense if one realizes that the Pt(-rich) clusters are small and long-range interactions play a major role in determining the work function. This seems somewhat surprising at first sight since the WF of clean and smooth Pt(111) (5.8 eV) is much larger than that of clean and smooth

DOI: 10.1021/acs.jpcc.6b11971
J. Phys. Chem. C 2017, 121, 8353−8363

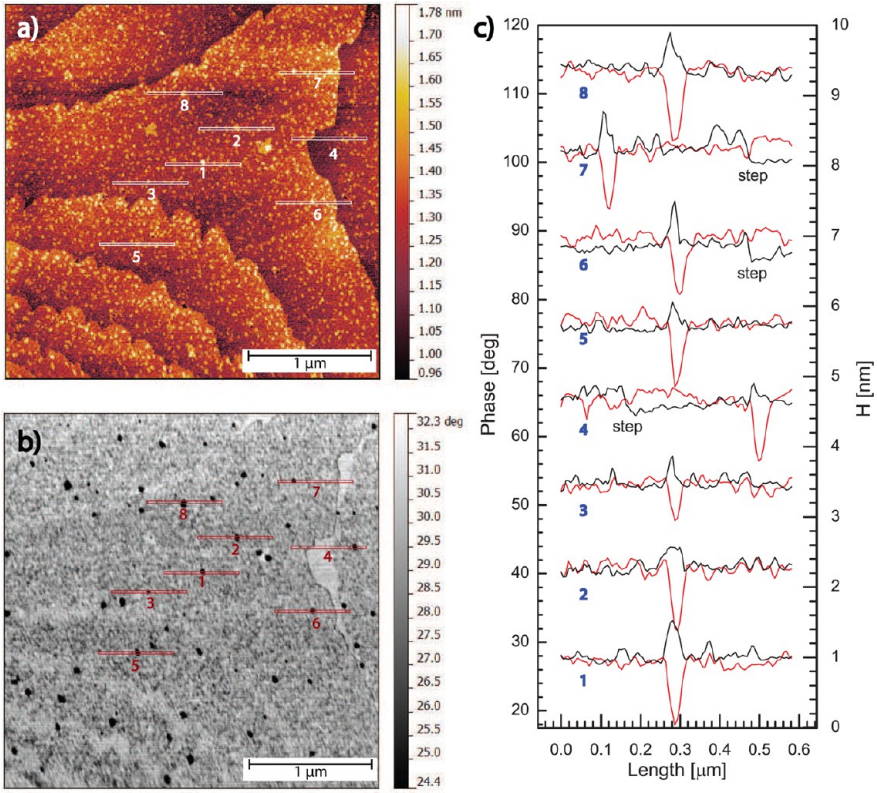

Figure 16. AFM images of 3 MLE Ag deposited on Pt(111) at 800 K and subsequently cooled to room temperature. (a) Topography image, (b) phase contrast image, and (c) typical line profiles through clusters obtained from phase contrast (red line) and topography (black line) image. The profiles have been shifted vertically for the sake of clarity.

Ag(111) (4.56 eV).[33] However, for the metals having fcc (face-centered-cubic) structure WF depends strongly on the surface orientation with a tendency for lower WF with decreasing coordination, i.e, $\phi_{111} > \phi_{100} > \phi_{110}$. This is even worse for amorphous dots with which we most likely deal here. Finite size effects may also lower the WF.[31] It is noted that field distortions around small objects make drawing clear conclusions hazardous. Therefore, we tentatively conclude that the case for Pt as the primary constituent of the clusters remains undecided on the basis of the current WF data.

A further increase of the coverage leads to a decrease of the average WF which at coverages of 1 and 2 MLE has the values $\Delta\phi = -1.085$ eV and $\Delta\phi = -1.33$ eV, respectively. The rather constant value of the WF beyond two-layer-thick films indicates that at most minor changes in topography and composition of the surface occur beyond a film thickness of two layers.

At a coverage of 3 MLE the average WF saturates at $\Delta\phi = -1.37$ eV. This saturation value is in the range reported by Härtel et al.[4] (−1.2 eV) and by Paffet et al.[2] (−1.5 eV) obtained at similar coverages. We note that the reported values were measured for the alloy formed after annealing the surface at 600 K. Schuster et al.[6] showed that both temperature and time during alloying drastically influence intermixing levels of the Ag/Pt(111) surface alloy, which results in different surface morphology leading to a variation in the surface WF. Moreover, the step density of the initial Pt(111) surface may have a decisive influence of several tenths of an electronvolt on the measured value.[34] In that respect, we can safely conclude that our data compare favorably with the macroscopic data available in the literature.

Characterization of 3 MLE Thick Film in Ambient AFM. To gain more insight on the composition and (if possible) structure of the black spots, we apply AFM. For that purpose we prepared a three-layer-thick Ag/Pt(111) film by deposition under ultrahigh vacuum (UHV) at 800 K as monitored by LEEM. As evident from Figure 14, and the discussion above, the surface predominantly consists of silver, but a substantial number of black spots are still observed. The AFM data have been taken in air at room temperature.

Figure 16 shows AFM data of the surface of the 3 MLE Ag/Pt(111) system grown in UHV (see above). The topography image of the surface presented in Figure 16a shows step contrast, which indicates that the surface is still flat. No pronounced geometric structures are observed. The phase contrast image presented in Figure 16b reveals the presence of many small, ∼50 nm wide, regions for which the measured phase shift is 10° lower than for the rest of the surface. We attribute these regions to the Pt clusters observed with LEEM as the number densities of the clusters obtained from the AFM and the LEEM images are very similar (8−15 clusters/μm^2) but their average size differs by about a factor of 2. The average size of clusters derived from the LEEM images is 120 nm, which is probably overestimated due to field distortion effects. From the typical height profiles shown in Figure 16c measured along the lines drawn in Figure 16a,b, we concluded that Pt clusters are about one to two layers higher than the surrounding layer. The phase shift contrast in the recorded images can be attributed to many factors;[27] nevertheless it points to the chemical composition of the clusters being different from the majority at the surface, which at 3 MLE is mainly composed of Ag atoms. We stress that the correlation between the phase

DOI: 10.1021/acs.jpcc.6b11971
J. Phys. Chem. C 2017, 121, 8353−8363

contrast and the height contrast is perfect. The black protrusions have a different chemical composition, and under the applied conditions probably oxidized Pt is the natural candidate. Therefore, the conclusion that the black dots consist of mainly platinum atoms is straightforward. The fact that the clusters protrude from the surface also explains the difficulty of selecting a proper focus condition in LEEM for these objects. We do believe that the footing of these clusters is still at the substrate and an oxygen layer contributes to the height differences.

A careful look at Figure 16b shows a pretty smooth edge on the upper terrace side of the ascending step edge. This is probably related to the initial step propagation growth mode.[35,36] The area has apparently a slightly different composition and or structure. We ascribe this feature to different possibilities of dealing with stresses near a descending step.

CONCLUSIONS

The spatiotemporal in situ information from LEEM on the growth of ultrathin Ag on Pt(111) at 750−800 K shows vivid and rich dynamic behavior. No significant differences were detected between the 750 and 800 K data. We confirm alloying and subsequent dealloying during the growth of the first monolayer at these elevated temperatures. Besides exchange processes between Ag and Pt occurring at steps, as reported earlier, direct alloying takes place on wide terraces. Initially alloying occurs and nucleation processes are prolonged as a result of increasingly reduced mobility of Ag and Pt adspecies on the alloying surface. New nucleation events are even observed at a coverage exceeding 70% of a monolayer! The adislands have a wide size distribution and are quite heterogeneous, especially the larger ones. Beyond a coverage of 50% of a monolayer a violent segregation of Pt toward the center of the islands occurs and bright Ag rims become apparent. Dealloying is fast during coalescence of the adatom islands. The remaining irregularly shaped vacancy islands are quickly filled by Pt(-rich) patches (black dots) and take a compact circular shape. These features are energetically favored since the integral step length is decreased and the boundaries between Pt(-rich) and Ag(-rich) areas are minimized. A concomitant transient relaxation of the exposed layer is inferred from the diffraction profiles. Upon further completion of the monolayer alloying reenters and the initial pseudomorphological structure is resumed as accompanied by reentrant (partial) alloying, which continues in the second layer.

The black dots are attributed to stressed, possibly amorphous Pt(-rich) features. Ex situ AFM experiments support this picture as the observed phase contrast images suggest chemical contrast. These Pt features persist even after deposition of several monolayers and probably have a firm base at the Pt substrate.

The here described features occur on wide terraces and are considered inherent to ultrathin Ag on ideal Pt(111). For narrow(er) terraces the exchange processes near steps will gain importance and may even dominate (see also ref 8).

Our present results are believed to apply for instance for ultrathin Ag films on the close packed heavy (4d and 5d) transition metal surfaces with an inherently high tensile surface tension. Similar observations might be made on the 3d transition metal (111) surfaces of Cu and Ni, but we mention that the all important tensile surface tension is a lot less strong in these cases.

ASSOCIATED CONTENT

Supporting Information

The Supporting Information is available free of charge on the ACS Publications website at DOI: 10.1021/acs.jpcc.6b11971.

LEEM movie recorded during deposition of the first Ag layer on Pt(111) surface at 750 K (ZIP)

Schematics of the alloying process of the first layer Ag/Pt(111) (PDF)

AUTHOR INFORMATION

Corresponding Author

*E-mail: maciej.jankowski@esrf.fr.

ORCID

Maciej Jankowski: 0000-0002-3796-0529

Present Address

†M.J.: ESRF—The European Synchrotron, 71 Avenue des Martys, Grenoble 38043, France.

Author Contributions

‡M.J. and E.V.: Both authors contributed equally to the presented work.

Notes

The authors declare no competing financial interest.

ACKNOWLEDGMENTS

We want to thank Robin Berkelaar for acquiring the AFM data. This work is part of ECHO research program 700.58.026, which is financed by the Chemical Sciences Division of The Netherlands Organisation for Scientific Research (NWO).

REFERENCES

(1) Davies, P.; Quinlan, M.; Somorjai, G. The growth and chemisorptive propertles of Ag and Au monolayers on platinum single crystal surfaces: An AES, TDS and LEED study. *Surf. Sci.* **1982**, *121*, 290−302.

(2) Paffett, M. T.; Campbell, C. T.; Taylor, T. N. Surface chemical properties of silver/platinum(111): comparisons between electrochemistry and surface science. *Langmuir* **1985**, *1*, 741−747.

(3) Röder, H.; Brune, H.; Bucher, J.-P.; Kern, K. Changing morphology of metallic monolayers via temperature controlled heteroepitaxial growth. *Surf. Sci.* **1993**, *298*, 121−126.

(4) Härtel, T.; Strüber, U.; Küppers, J. Growth and properties of thin Ag films on Pt(111) surfaces. *Thin Solid Films* **1993**, *229*, 163−170.

(5) Grossmann, A.; Erley, W.; Hannon, J. B.; Ibach, H. Giant Surface Stress in Heteroepitaxial Films: Invalidation of a Classical Rule in Epitaxy. *Phys. Rev. Lett.* **1996**, *77*, 127−130.

(6) Schuster, R.; Roder, H.; Bromann, K.; Brune, H.; Kern, K. Stress relief via island formation of an isotropically strained bimetallic surface layer: The mesoscopic morphology of the Ag/Pt (111) surface alloy. *Phys. Rev. B: Condens. Matter Mater. Phys.* **1996**, *54*, 13476−13479.

(7) Becker, A. F.; Rosenfeld, G.; Poelsema, B.; Comsa, G. Two-dimensional microstructures of submonolayer Ag on Pt(111) induced by elastic strain. *Phys. Rev. Lett.* **1993**, *70*, 477−480.

(8) Röder, H.; Schuster, R.; Brune, H.; Kern, K. Monolayer-confined mixing at the Ag-Pt(111) interface. *Phys. Rev. Lett.* **1993**, *71*, 2086−2089.

(9) Strüber, U.; Küppers, J. Spectroscopic confirmation of STM derived Ag/Pt mixing in annealed Ag submonolayers at Pt(111) surfaces. *Surf. Sci.* **1993**, *294*, L924−L928.

(10) Bendounan, A.; Braun, J.; Minár, J.; Bornemann, S.; Fasel, R.; Gröning, O.; Fagot-Revurat, Y.; Kierren, B.; Malterre, D.; Sirotti, F.; et al. Monitoring the formation of interface-confined mixture by photoelectron spectroscopy. *Phys. Rev. B: Condens. Matter Mater. Phys.* **2012**, *85*, 245403.

DOI: 10.1021/acs.jpcc.6b11971
J. Phys. Chem. C 2017, 121, 8353−8363

(11) Zeppenfeld, P.; Krzyzowski, M.; Romainczyk, C.; Comsa, G.; Lagally, M. G. Size relation for surface systems with long-range interactions. *Phys. Rev. Lett.* **1994**, *72*, 2737−2740.
(12) Zeppenfeld, P.; Krzyzowski, M.; Romainczyk, C.; David, R.; Comsa, G.; Röder, H.; Bromann, K.; Brune, H.; Kern, K. Stability of disk and stripe patterns of nanostructures at surfaces. *Surf. Sci.* **1995**, *342*, L1131−L1136.
(13) Tersoff, J. Surface-confined alloy formation in immiscible systems. *Phys. Rev. Lett.* **1995**, *74*, 434−437.
(14) Jankowski, M.; Wormeester, H.; Zandvliet, H. J. W.; Poelsema, B. Desorption of oxygen from alloyed Ag/Pt(111). *J. Chem. Phys.* **2014**, *140*, 234705.
(15) Diemant, T.; Schüttler, K. M.; Behm, R. J. Ag on Pt (111): Changes in electronic and CO adsorption properties upon PtAg/Pt (111) monolayer surface alloy formation. *ChemPhysChem* **2015**, *16*, 2943−2952.
(16) Schüttler, K.; Mancera, L.; Diemant, T.; Groß, A.; Behm, R. Interaction of CO with Pt x Ag 1- x/Pt (111) surface alloys: More than dilution by Ag atoms. *Surf. Sci.* **2016**, *650*, 237−254.
(17) Brune, H.; Röder, H.; Boragno, C.; Kern, K. Strain relief at hexagonal-close-packed interfaces. *Phys. Rev. B: Condens. Matter Mater. Phys.* **1994**, *49*, 2997−3000.
(18) Aït-Mansour, K.; Brune, H.; Passerone, D.; Schmid, M.; Xiao, W.; Ruffieux, P.; Buchsbaum, A.; Varga, P.; Fasel, R.; Gröning, O. Interface-confined mixing and buried partial dislocations for Ag bilayer on Pt(111). *Phys. Rev. B: Condens. Matter Mater. Phys.* **2012**, *86*, 085404.
(19) Jankowski, M.; Wormeester, H.; Zandvliet, H. J. W.; Poelsema, B. Temperature-dependent formation and evolution of the interfacial dislocation network of Ag/Pt(111). *Phys. Rev. B: Condens. Matter Mater. Phys.* **2014**, *89*, 235402.
(20) Hlawacek, G.; Jankowski, M.; Wormeester, H.; van Gastel, R.; Zandvliet, H. J. W.; Poelsema, B. Visualization of steps and surface reconstructions in Helium Ion Microscopy with atomic precision. *Ultramicroscopy* **2016**, *162*, 17−24.
(21) Brune, H.; Giovannini, M.; Bromann, K.; Kern, K. Self-organized growth of nanostructure arrays on strain-relief patterns. *Nature* **1998**, *394*, 451−453.
(22) Aït-Mansour, K.; Ruffieux, P.; Xiao, W.; Gröning, P.; Fasel, R.; Gröning, O. C 60 on strain-relief patterns of Ag/ Pt (111): Film orientation governed by template superstructure. *Phys. Rev. B: Condens. Matter Mater. Phys.* **2006**, *74*, 195418.
(23) Aït-Mansour, K.; Buchsbaum, A.; Ruffieux, P.; Schmid, M.; Gröning, P.; Varga, P.; Fasel, R.; Gröning, O. Fabrication of a Well-Ordered Nanohole Array Stable at Room Temperature. *Nano Lett.* **2008**, *8*, 2035−2040.
(24) Aït-Mansour, K.; Treier, M.; Ruffieux, P.; Bieri, M.; Jaafar, R.; Gröning, P.; Fasel, R.; Gröning, O. Template-directed molecular nanostructures on the Ag/Pt (111) dislocation network. *J. Phys. Chem. C* **2009**, *113*, 8407−8411.
(25) Aït-Mansour, K.; Ruffieux, P.; Gröning, P.; Fasel, R.; Gröning, O. Positional and orientational templating of C60 molecules on the Ag/Pt (111) strain-relief pattern. *J. Phys. Chem. C* **2009**, *113*, 5292−5299.
(26) Linke, U.; Poelsema, B. A simple procedure for high precision orientation of single crystal surfaces. *J. Phys. E: Sci. Instrum.* **1985**, *18*, 26−27.
(27) García, R.; Magerle, R.; Perez, R. Nanoscale compositional mapping with gentle forces. *Nat. Mater.* **2007**, *6*, 405−411.
(28) Pentcheva, R.; Fichthorn, K. A.; Scheffler, M.; Bernhard, T.; Pfandzelter, R.; Winter, H. Non-Arrhenius Behavior of the Island Density in Metal Heteroepitaxy: Co on Cu(001). *Phys. Rev. Lett.* **2003**, *90*, 076101.
(29) Uchida, Y.; Lehmpfuhl, G. Estimation of ad-vacancy formation energy on the Pt(111) surface by using reflection electron microscopy. *Surf. Sci.* **1991**, *243*, 193−198.
(30) Venables, J. Metal nucleation and growth on insulating substrates. *Introduction to Surface and Thin Film Processes*; Cambridge University Press: Cambridge, U.K., 2000.
(31) Nepijko, S. A.; Sedov, N. N.; Schönhense, G. Peculiarities of imaging one- and two-dimensional structures using an electron microscope in the mirror operation mode. *J. Microsc.* **2001**, *203*, 269−276.
(32) Besocke, K.; Krahl-Urban, B.; Wagner, H. Dipole moments associated with edge atoms; A comparative study on stepped Pt, Au and W surfaces. *Surf. Sci.* **1977**, *68*, 39−46.
(33) Kawano, H. Effective work functions for ionic and electronic emissions from mono- and polycrystalline surfaces. *Prog. Surf. Sci.* **2008**, *83*, 1−165.
(34) Poelsema, B.; Palmer, R. L.; Comsa, G. Helium scattering and work function investigation of co adsorption on Pt(111) and vicinal surfaces. *Surf. Sci.* **1982**, *123*, 152−164.
(35) Jankowski, M. Reciprocal and real space investigation of Ag/Pt (111): growth, structure and interaction with oxygen. Ph.D. Thesis, Universiteit Twente, 2014.
(36) van Vroonhoven, E. Remarkable Interface Activity: A LEEM Study of Ge(001) and Ag/Pt(111) at High Temperatures. Ph.D. Thesis, University of Twente, 2005.

DOI: 10.1021/acs.jpcc.6b11971
J. Phys. Chem. C 2017, 121, 8353−8363